SFF 2021 Paper- Non-Review submission

Predict Adhesive Strength of Repair of Thermoplastic Component Based on Polymer Healing Theory

Charul Chadha[1], Albert E. Patterson[2,3], Iwona Jasiuk[1]

[1]Department of Mechanical Science and Engineering
[2]Department of Industrial and Enterprise Systems Engineering
[3]Department of Engineering Technology and Industrial Distribution, Texas A&M University
The University of Illinois at Urbana-Champaign, Urbana, Illinois 61801

† Correspondence: charulc2@illinois.edu

ABSTRACT:

Advancements in polymer technology have increased the production of high-valued parts using polymers. These parts are often produced in low volumes and have complex geometries, making them difficult to reproduce later, especially when original tooling is no longer available. Reproduction of these parts from scratch using additive manufacturing (AM) can be time-consuming and, at times, economically infeasible. This paper explores the application of fused filament fabrication (FFF-extrusion-based AM) to repair such parts and print broken features on damaged parts. Polymer healing theory is then employed to understand the effect of print speed on adhesive strength at the interface formed between the 3D printed repair geometry and the original damaged part. The theory was verified using three-point bending experiments. Results show that the adhesive strength at the interface is approximately proportional to print speed raised to power negative one-fifth fraction.

1. Introduction

3D printing, a subset of additive manufacturing (AM), is one of the most steadily increasing manufacturing technologies. AM has unique capabilities to print intricate details, complex geometries, and near net components [1]. It can also improve supply chain processes as it does not need complicated toolings, can print a variety of materials, can manufacture components on demand, and readily print customized designs. As a result, studies have shown that the inclusion of AM in areas other than manufacturing (maintenance, repair, and overhaul strategies) can significantly improve the supply chain process [2–5].

To print a part using AM, a computer-aided design (CAD) model is generated first. The CAD model is then transferred to a slicer software that cuts the model into layers. A G-code is generated for each layer that is fed into the 3D printer. The printer then deposits material in layers, and after completion of each layer, either the print bed moves down, or the extruder head moves up according to the layer height. Several different types of AM processes are available on the market that can print a variety of materials. These processes are broadly classified into one of the seven categories: binder jetting, material jetting, direct energy deposit, VAT photopolymerization,

powder bed fusion, sheet lamination, and material extrusion [34] In the current study, we focus on the application of fused filament fabrication (FFF) to repair polymeric components, which is a type of material extrusion AM.

In FFF, thermoplastic materials are fed into the heated extruder head, which increases the material's temperature above its glass transition temperature. The heated material is then deposited on the print bed or existing material in a layer-by-layer fashion. Since the material is deposited in AM process instead of subtracting it (as in traditional manufacturing processes), it can be used to repair components by adding material at the failure location. Several studies have investigated the repair of metallic parts using different AM processes [6–14]. However, there is still a lack of understanding on how to repair components using FFF. In a prior study, the authors demonstrated that FFF could be used to repair thermoplastic components [15]. In another study, Richter et al. [16] investigated the effect of surface preparation and nozzle distance on repairing ABS and polypropene (PP) by directly depositing the material on respective molded sheets using FFF. They found that decreasing the nozzle distance from the deposition surface improves the bond strength. In contrast, surface preparation had a negligible effect. In another study, Wits et al. [3] studied the application of FFF for repair and overhaul strategies. However, they printed a re-designed component from scratch for the repair process instead of repairing the damaged part.

Though previous studies have shown that FFF can be used to repair polymeric components, these studies do not investigate the effect of different printing parameters on the adhesive strength of the deposited material. For an effective repair, a strong adhesive bond should be formed between the deposited material and the damaged part so that the stresses can be efficiently distributed at the repaired location without delaminating the deposited material at the interface. In this paper, we study the effect of print speed on the adhesive strength of the repair interface. Patches were printed directly on top of the pre-cracked acrylonitrile butadiene styrene (ABS) bars using FFF at different speeds. The repaired bars were then tested under three-point bending, and the maximum load at failure for each was recorded. Polymer healing theory was then used to describe the observations. Modified equation based on the equation formed by Wool and O-Conner[17,18] was fitted to obtain an analytical solution to predict adhesive strength of the deposited polymers at different speeds. The paper is divided into eight sections. A basic introduction is provided in section 1. Polymer healing theory is briefly discussed in section 2, followed by a literature review on how the concepts derived from the theory have been used for FFF. Modified equation (derived from polymer healing theory) is then introduced in section 3. Sections 4 and 5 describe the steps undertaken to prepare samples for three-point bending and the experimental setup. The results obtained from the experiments are provided in section 6, followed by a discussion in section 7. Finally, the conclusions and future work are described in section 8.

2. Literature review

In unpublished work, the authors found that the adhesive strength of the deposited material can be described by polymer healing theory. The theory, initially developed by Wool and O'Conner in 1981 [17,18,] is based on the reptation model developed by De Gennes [19]. This microscopic theory relates the restoration of mechanical properties (stress, strain, modulus, and impact energy) to time,

temperature, pressure, molecular weight, and material constitution. According to this theory, when two pieces of amorphous polymers are brought in contact above their glass transition temperature, the polymer chains at the interface gradually penetrate each other. Suppose the interface is kept above the glass transition temperature for a long time. In that case, the interface gradually heals and eventually becomes indistinguishable from the bulk material. At this stage, the interface demonstrates the material's bulk properties, and the material is said to be healed.

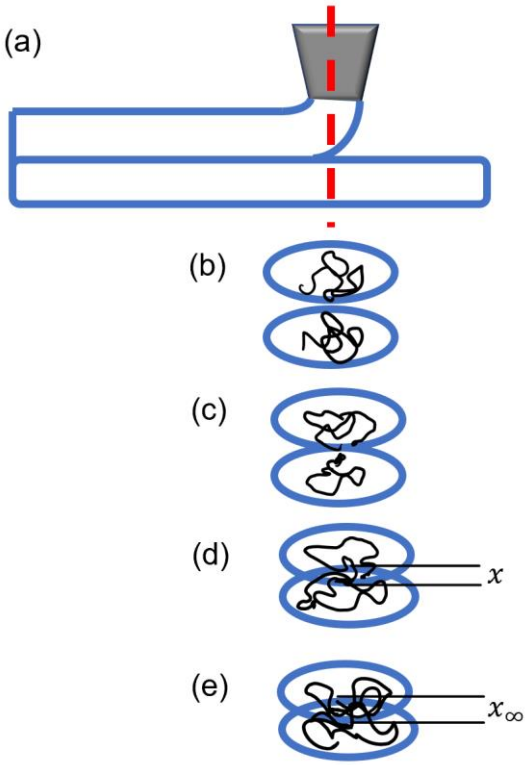

Figure 1: Five steps of polymer healing a) Deposition of polymer in FFF, b) Surface approach and surface rearrangement, c) Wetting, d) Interpenetration to a distance x, e) interpenetration to an equilibrium distance x_∞

Complete healing of the polymer interface is achieved in five steps: surface approach, surface rearrangement, wetting, interpenetration to a distance x, and finally interpenetration to an equilibrium distance x_∞[20], as shown in Figure 1 (b-e). In the first two stages of the theory, when the polymers are heated above the glass transition temperature, the polymer chains at the surface begin to rearrange themselves. Then, the morphology and topology of the surface begin to change when they are bought in contact due to chemical reactions, smoothening of crests, turfs (and so on). Once the first two stages are accomplished, the polymeric chains of the two surfaces are in contact and begin to attract each other. This step is described as wetting of the polymer. Once wetting is accomplished, the polymeric chains start diffusing into each other. As a result, polymeric chains penetrate the surface and entangle with the chains available at the adjacent surface. The penetration of the chains increases with time. As a result, when the interface (two surfaces) is kept above glass transition temperature for a long time (reptation time t_r), the virgin properties of the

bulk material are restored at the surface. For a large surface, different areas may be at different stages described by the polymer healing theory.

Based on the healing theory, at a given time *t* (less than reptation time), the recovery in the strength of the interface can be described by equation (1)[18]

$$R(\sigma,t) = \left[R_0 + \left(\frac{K}{\sigma_\infty} t^{1/4} \dot{\psi}(t)\right)\right] \phi(t) \qquad (1)$$

where *t* is the time at which the interface is kept above the glass transition temperature. *R* is the recovery ratio of stress compared to virgin material. R_0 is the ratio of yield stress due to attraction of wetting surface (σ_0) to yield stress at of virgin material (σ_∞). *K* is a constant, $\psi(t)$ is diffusion initiation function, and $\phi(t)$ is wetting distribution function.

If instantaneous wetting is assumed throughout the contact area, then $\psi(t)$ and $\phi(t)$ are equal to one. Equation (1) can then be rearranged as:

$$R(\sigma,t) = \frac{\sigma_o}{\sigma_\infty} + \frac{K}{\sigma_\infty} t^{1/4} \qquad (2)$$

From equation (2), we obtain

$$\sigma \sim t^{\frac{1}{4}}$$

$$\frac{\sigma}{\sigma_\infty} = \left(\frac{t}{t_\infty}\right)^{1/4} \qquad (3)$$

Equation (3) is a commonly used equation to predict the welding strength of amorphous polymers [20] and has been used to predict bond strength between deposited filament material in FFF.

Due to significant technical advancement in FFF in the last decade (like Big Area Additive Manufacturing and printing of composite materials), interest in understanding and predicting bond strength of the deposited material has gained considerable attention. The bond strength in literature has been predicted in one of the two ways: using sintering models (predicting the necking growth between the deposited filaments) [21–26] or analyzing and developing equations to predict the diffusion of polymeric chains [24,27–32]. While using a sintering model to predict bond strength, it is assumed that higher growth in the necking area will result in stronger bond strength. However, sintering models only provide information about surface contact and wetting. They do not provide direct information about the diffusion of molecules across the interface or if the interface has achieved the bulk properties. According to polymer healing theory, the interfacial bond strength can continue to grow once the surface contact has occurred.

3. Adaptation of polymer healing theory for FFF

In the FFF method, the time at which the material is kept above the glass transition temperature cannot be directly controlled. Instead, it can be indirectly controlled using a print speed as the speed equals distance divided by time. Substituting this relation in equations (3):

$$\frac{\sigma}{\sigma_\infty} = \left(\frac{S_\infty}{S}\right)^{1/4} \quad (4)$$

In the case of FFF, although the relationship described by equations (2) and (3) has been used, equation (4) should not be used in the same format because:

1) The equation assumes the wetting distribution function equal to one, which is not valid in the case of FFF as the contact area between deposited filament material can increase with time [23].
2) The equation assumes that the interface is kept above a critical penetration temperature for a constant period of time. However, in FFF, the deposited material is subjected to repeated heating and cooling as a heated nozzle moves above it.
3) The temperature profile of deposited filament material is non-isothermal.

Thus, a more general relation that considers the assumptions mentioned above is given as follows

$$\frac{\sigma}{\sigma_\infty} = \left(\frac{S_\infty}{S}\right)^{1/n} \quad (5)$$

where *n* is a constant. Taking the log of equation (5) and rearranging the terms, we get

$$\ln(\sigma) = \frac{-1}{n}\ln(S) + C \quad (6)$$

where *C* is a constant. Thus, from equation (6), one can find the adhesive strength of the interface at failure for a given speed provided *n* is known.

4. Sample preparation

ABS bars of dimensions 203 mm x 9.5 mm x 25.4 mm supplied by McMaster Carr were purchased for preparing the samples. These ABS bars acted as the base material for printing. A 4 mm deep notch was milled at the center of the bar using a 60˚router bit with a 0.2 mm tip to simulate failure in the material. The notches were then pre-cracked using a desktop pre-cracking device (Figure 2). The details of the device are described elsewhere 33. The samples were then left at ambient temperature for forty-eight hours, after which the patches from ABS filament of diameter 0.75 mm, supplied by hatchbox were printed. The printed patches had dimensions of 25.4 mm x 25.4 mm x 5 mm. Two modifications were made to the printer to print the patches on existing material. Firstly, a jig was secured to the print bed using nuts and screws. The jig held the bars in place during the printing operation. Secondly, an attachment consisting of a body and screw was attached to the rails of the printer to offset the z axis, as shown in Figure 3. It was necessary to add offset in the z-axis to compensate for the height of the bar as it was placed on a jig above the print bed. The offset was precisely controlled using the extension of the screw, such that the z = 0 plane defined in the G-code lie above the surface to be printed for each bar.

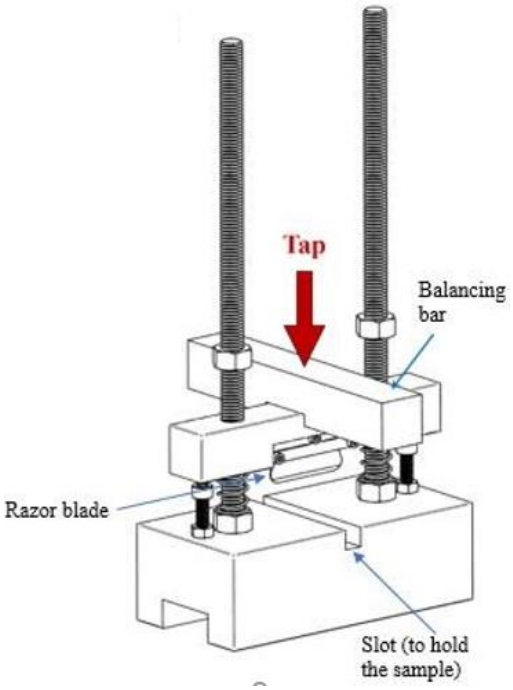

Figure 2: Desktop pre-cracking device used to create pre-cracks [33]

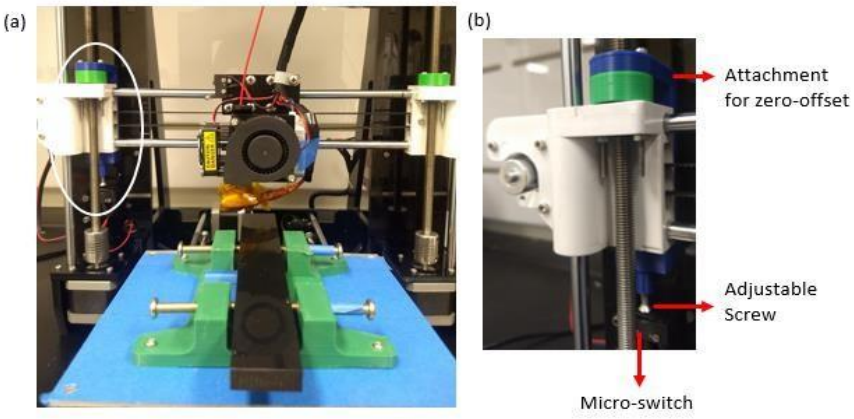

Figure 3 a) Jig attached to the print bed to secure ABS bars b) Attachment to adjust the z-axis of the machine.

Once the pre-cracked ABS bars were secured in the jig, the top surface was thoroughly cleaned with isopropyl alcohol to remove impurities. Once the alcohol evaporated, the patches were printed using the G-code developed by Cura software. During the generation of the G-code, all the printing parameters except for the print speed were kept constant. The different print speeds were used in the study: 10 mm/s, 20 mm/s, 40 mm/s, and 60 mm/s. Table 1 shows the printing parameters used for the patches. Figure 4 shows the sample after the patches were printed on it.

Figure 4: Sample after printing patches on both sides

5. Experimental results

Once the patches were printed on both sides of the bars, the samples were left at ambient conditions for over forty-eight hours before being tested under three-point bending. The load was applied at specimen's center at the 1.5 mm/min rate for three-point bending, and the span length was 150 mm. The maximum load before failure was noted for each sample and is presented in Table 2. Five bars were tested to establish the baseline for the tests (i.e. determine the load carrying capacity of the bars before failure without patches). Five and three specimens were tested for the samples with the patch print speed of 60 mm/s and 10 mm/s, respectively. Five test specimens were initially tested for print speeds 40 mm/s and 20 mm/s; however, one observation with high deviation from mean was recorded at both speeds. Thus, a sixth sample was also tested for these two print speeds.

Table 2: Maximum force at failure under three-point bending for different samples

	Sample No.	Baseline	60 mm/s	40 mm/s	20 mm/s	10 mm/s
Maximum force at failure (kN)	1	0.946	1.68	1.81	2.16	2.18
	2	0.878	1.67	1.89	1.87	2.16
	3	0.971	1.49	1.59	1.75	2.18
	4	0.965	1.41	1.62	1.74	-
	5	0.949	1.51	1.22	1.78	-
	6	-	-	1.73	1.62	-

6. Results

6.1 Modes of failure

When loaded in three-point bending, the samples failed in one of the two ways: adhesive failure or substrate failure. The two types of failure are shown in Figure 5. Adhesive failure was the most common type of failure observed. In this failure, the printed patches were delaminated from the bars. Once the patches were delaminated, the crack propagated from the pre-crack, as seen in Figure 5a. These failures were observed for patches printed at print speeds 60 mm/s, 40 mm/s, and 20 mm/s. Substrate failure was only observed at 10 mm/s. In substrate failure, the patches did not delaminate. Instead, the crack found another location to initiate, causing the material failure. All

the samples printed at print speed 10 mm/s failed through a substrate failure. This is an interesting finding as we do not expect the adhesive strength of the printed material to be stronger than the base material. A plausible explanation for the substrate failure can be that the patches and ABS bars acted as a single material, which increased the moment of inertia of the sample under the point of loading. However, since the patches had sharp corners, a stress concentration was developed at the corner, promoting the substrate to fail at this location instead.

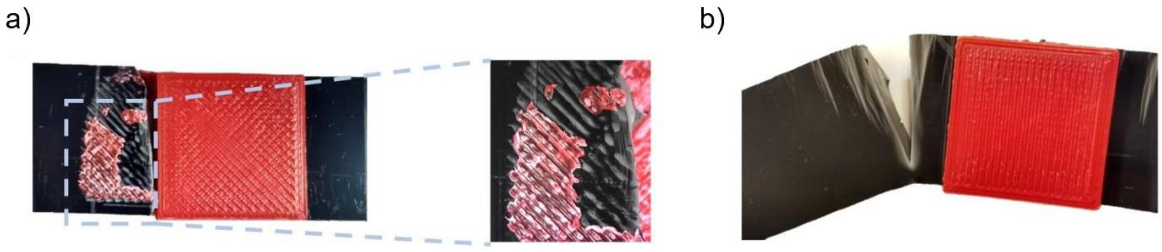

Figure 5: Two modes of failure observed during three-point bending a) Adhesive failure b) Substrate failure

6.2 Grubb test

While analyzing the maximum force at failure, two observations (one for 40 mm/s and one at 20 mm/s) stood out as they had a high deviation from the mean values. Grubb tests with alpha 0.05 were done to determine if they were an outlier. Table 3 shows calculations for 40 mm/s whereas Table 4 shows calculations for 20 mm/s. The mean was calculated by taking the average values of all observations. The standard deviation and z score were calculated using the following equations:

$$s = \sqrt{\frac{\sum_{i=1}^{n}(x_i - X_{mean})^2}{n-1}}$$

$$z = \frac{|x_i - X_{mean}|}{s}$$

Table 3: Grubb Test calculations at 40 mm/s

Sample No.	40 mm/s	z
1	1.81	0.7054
2	1.89	1.0422
3	1.59	0.2211
4	1.62	0.0947
5	1.22	1.7960
6	1.73	0.3643
Mean	1.6425	
s	0.2375	

Table 4: Grubb Test calculations at 20 mm/s

Sample No.	20mm/s	z
1	2.16	1.8488
2	1.87	0.2425
3	1.75	0.3795
4	1.74	0.4336
5	1.78	0.2064
6	1.62	1.0718
Mean	1.822	
SD	0.184898	

From the Grubb test, the p-value for sample number 5 printed at 40 mm/s is 0.128, and sample 1 printed at 20 mm/s is 0.086. Since for both print speeds, *p* is greater than 0.05, the samples cannot be concluded as outliers. However, the Grubb test has inherited assumptions, and due to the small sample size, one cannot conclude with high confidence that all the assumptions are met. Thus, while calculating results, two sets of data are assumed—one with all the observation values and one after removing the two values of concern.

6.3 Removing the two observations:

Mean values for the max force at failure were calculated after removing two measurements of concern (sample 1 printed at 20 mm/s and sample 5 printed at 40 mm/s). The natural log of both mean values and print speed was then calculated and plotted in Figure 6. A linear line was then fitted. The R^2 value of the equation obtained through linear regression was 0.8891. Comparing equation six with the linear regression equation shown in Figure 6, *n* equals 5.26.

Table 5 Print speed and mean of the maximum force at failure (not considering two observations)

S.No.	Print Speed (s)	Mean max force (f)	ln(s)	ln(f)
	mm/s	kN		
1	60	1.55	4.09	0.44
2	40	1.73	3.69	0.55
3	20	1.75	3.00	0.56
4	10	2.17	2.30	0.78

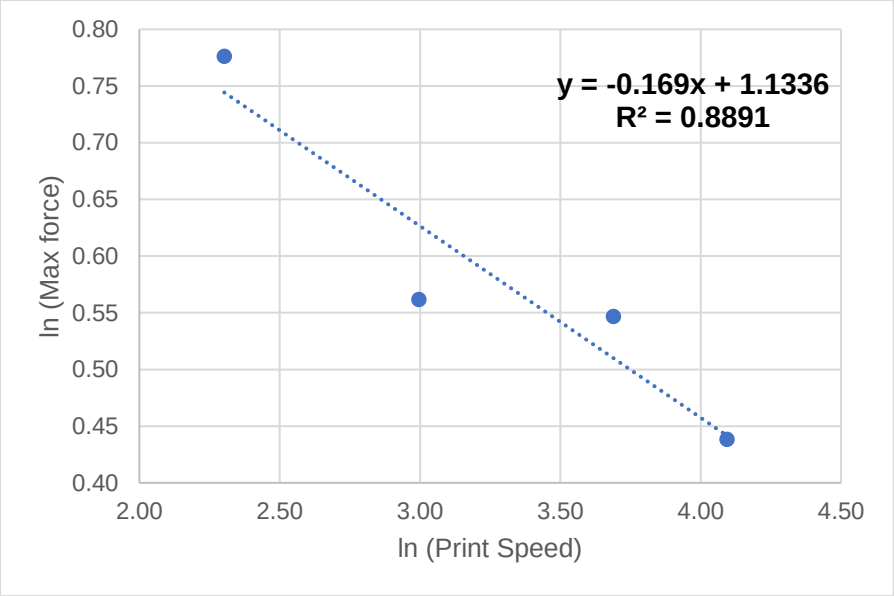

Figure 6: Log of print speed v/s maximum force at failure when two observations are not included

6.4 Including all observations

A similar procedure described in Section 6.2 is followed. Considering all observations, we get the mean values described in Table 6. The logarithmic valued obtained in Table 6, when fitted to the linear regression model, gives the equation shown in Figure 7, which, when compared to equation 6, gives n= 5.3966.

Table 6 Print speed and mean of the maximum force at failure (considering all observations)

S.No.	Print Speed (s)	Mean max force (f)	ln(s)	ln(f)
	mm/s	kN		
1	60	1.55	4.09	0.44
2	40	1.64	3.69	0.50
3	20	1.82	3.00	0.60
4	10	2.17	2.30	0.78

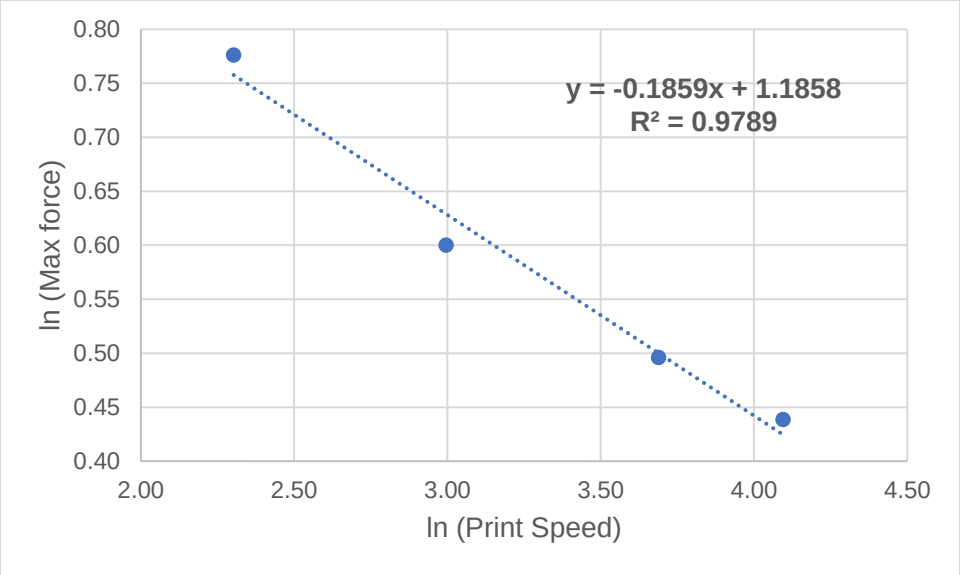

Figure 7: Log of print speed v/s maximum force at failure when all observations are included

7 Discussion

The general observations are inferred using Table 2 and Table 5. From the maximum force at failure in these two tables, we can notice that the samples in which no patches were printed (baseline) failed before the samples in which the patches were printed. The delay in the failure in the presence of patches is because additional energy is consumed to delaminate the patches or find a new site for crack initiation (in the case of print speed 10 mm/s). Thus, one can safely assume that this strategy can be used to prolong the operating life of the equipment if high tolerance is not required. When high tolerances are necessary, the damaged area can be first machined and then filled (provided the extruder nozzle can reach the print area).

We also observe that the maximum force at failure increases with a decrease in print speed. This inverse relationship can be explained by the polymer healing theory. As the print speed decreases, the rate at which the print nozzle passes through a given point decreases. Since the nozzle is above the material's glass transition temperature, the rate of dissipation of heat for the deposited material reduces. As a result, the interface is at a higher temperature for a longer duration enabling cross-over and entanglement of additional polymer chains.

Another interesting observation made from Table 2 is that the ranges of maximum force at failure for print speeds 40 mm/s and 20 mm/s overlap with each other to a greater extent. Considerable overlap between the two ranges can be attributed to high standard deviation. The reasons for the large standard deviation at the two print speeds are unknown and need to be investigated further. In contrast, the maximum force at failure for the print speed of 10 mm/s is approximately consistent. High consistency is observed at 10 mm/s because all samples printed at 10 mm/s failed at substrate, thus the load at failure are governed by the material properties of ABS bar. Since all

the samples failed in the substrate for 10 mm/s, it can be safely assumed that complete polymer healing took place at this print speed.

From the results obtained in Sections 6.2 and 6.3, we can assume that for FFF, the relationship between the adhesive strength of the deposited material and print speed can be expressed as power-law described by equation (5). The exponent *n* in the case of FFF for ABS material lies between 5.39 to 5.26. Variations observed in obtaining a maximum force at failure need to be reduced, or the sample size of the experiments should be increased to reduce range of *n*.. However, we can conclude that the exponent is greater than four, and the direct relation derived from polymer healing theory, described by equation (3), is not valid for FFF. As discussed in Section 3, this can be due to either repeated heating and cooling observed by the material during the printing process or dependence of the wetting distribution function on time.

8 Conclusions

The bond strength of the deposited polymer in FFF can be determined using polymer healing theory. However, the traditional equations derived to predict bond strength at the interface of the deposited polymer in the case of polymer welding are based on the time at which the interface is maintained above the glass transition temperature. Since we can not control this time directly in FFF, a modified equation relating print speed to bond strength was derived. According to this analytical equation, the adhesive strength can be related to print speed using an inverse power law. The exponent of the inverse power law was determined experimentally using three-point bending. To prepare samples for three-point bending, patches was printed directly over pre-cracked ABS bas on either side. When loaded under three-point bending, the maximum force at failure for each bar was noted. Based on the results obtained, we conclude that

- As print speed increases, the adhesive strength increases.
- Since the patches printed at the print speed of 10 mm/s did not delaminate, we infer that complete polymer welding can be achieved in FFF at critical print speed.
- The print speed and adhesive strength of the material follow the following relationship:

$$\frac{\sigma}{\sigma_\infty} = \left(\frac{S_\infty}{S}\right)^{1/n}$$

where σ_∞ is the strength of virgin material, S_∞ is critical print speed, S is the print speed of the component, σ is adhesive strength, and n is a constant, for ABS n lies between 5.26-5.39.

In the current study, both print temperature and material were constant. However, to validate the generality of the derived equation, it should be validated at different print temperatures and other amorphous materials.

9. References

1. Ngo TD, Kashani A, Imbalzano G, Nguyen KTQ, Hui D. Additive manufacturing (3D printing): A review of materials, methods, applications and challenges. *Compos Part B Eng*. 2018;143. doi:10.1016/j.compositesb.2018.02.012

2. Thomas D. Costs, benefits, and adoption of additive manufacturing: a supply chain

perspective. *Int J Adv Manuf Technol*. 2016;85(5-8). doi:10.1007/s00170-015-7973-6

3. Wits WW, García JRR, Becker JMJ. How Additive Manufacturing Enables more Sustainable End-user Maintenance, Repair and Overhaul (MRO) Strategies. *Procedia CIRP*. 2016;40. doi:10.1016/j.procir.2016.01.156

4. Khajavi SH, Partanen J, Holmström J. Additive manufacturing in the spare parts supply chain. *Comput Ind*. 2014;65(1). doi:10.1016/j.compind.2013.07.008

5. Guo N, Leu MC. Additive manufacturing: technology, applications and research needs. *Front Mech Eng*. 2013;8(3). doi:10.1007/s11465-013-0248-8

6. Gasser A, Backes G, Kelbassa I, Weisheit A, Wissenbach K. Laser additive manufacturing: laser metal deposition (LMD) and selective laser melting (SLM) in turbo-engine applications. *Laser Tech J*. 2010;7(2). doi:10.1002/latj.201090029

7. Portolés L, Jordá O, Jordá L, Uriondo A, Esperon-Miguez M, Perinpanayagam S. A qualification procedure to manufacture and repair aerospace parts with electron beam melting. *J Manuf Syst*. 2016;41. doi:10.1016/j.jmsy.2016.07.002

8. Koehler H, Partes K, Seefeld T, Vollertsen F. Influence of Laser Reconditioning on Fatigue Properties of Crankshafts. *Phys Procedia*. 2011;12. doi:10.1016/j.phpro.2011.03.063

9. Liu Z, Jiang Q, Li T, et al. Environmental benefits of remanufacturing: A case study of cylinder heads remanufactured through laser cladding. *J Clean Prod*. 2016;133. doi:10.1016/j.jclepro.2016.06.049

10. Wilson JM, Piya C, Shin YC, Zhao F, Ramani K. Remanufacturing of turbine blades by laser direct deposition with its energy and environmental impact analysis. *J Clean Prod*. 2014;80. doi:10.1016/j.jclepro.2014.05.084

11. Kattire P, Paul S, Singh R, Yan W. Experimental characterization of laser cladding of CPM 9V on H13 tool steel for die repair applications. *J Manuf Process*. 2015;20. doi:10.1016/j.jmapro.2015.06.018

12. Saurabh S. Direct numerical simulation of human phonation. Published online 2017. http://hdl.handle.net/2142/99180

13. Brooks R. Researchers Developing 3D Printing for Die Repair. *Foundry management & Technology*. March 25, 2013.

14. Mudge RP, Wald NR. Laser Engineered Net Shaping Advances Additive Manufacturing and Repair. *Weld J*. 2007;86(1):44-48.

15. Chadha C, Patterson AE, Allison JT, James KA, Jasiuk IM. Repair of high-value plastic components using fused deposition modeling. In: *30th Annual International Solid Freeform Fabrication Symposium - An Additive Manufacturing Conference*. Solid Freeform Fabrication Symposium – An Additive Manufacturing Conference; 2019:1732-1755.

16. Richter A, Kessing D, Fischer F, Pelzer L, Dilger K. Print-On Strategies to Bond Injection

Molded Parts with Structures Produced by Fused-Deposition-Modeling. *Proc Des Soc Int Conf Eng Des*. 2019;1(1). doi:10.1017/dsi.2019.86

17. Wool RP, O'Connor KM. Time dependence of crack healing. *J Polym Sci Polym Lett Ed*. 1982;20(1). doi:10.1002/pol.1982.130200102

18. Wool RP, O'Connor KM. A theory crack healing in polymers. *J Appl Phys*. 1981;52(10). doi:10.1063/1.328526

19. de Gennes PG. Reptation of a Polymer Chain in the Presence of Fixed Obstacles. *J Chem Phys*. 1971;55(2). doi:10.1063/1.1675789

20. Wool RP, Yuan B-L, McGarel OJ. Welding of polymer interfaces. *Polym Eng Sci*. 1989;29(19). doi:10.1002/pen.760291906

21. Li L, Sun Q, Bellehumeur C, Gu P. Investigation of Bond Formation in FDM Process. In: *Solid Freeform Fabrication Symposiun*. ; 2001:1-8.

22. Sun Q, Rizvi GM, Bellehumeur CT, Gu P. Effect of processing conditions on the bonding quality of FDM polymer filaments. *Rapid Prototyp J*. 2008;14(2). doi:10.1108/13552540810862028

23. Bellehumeur C, Li L, Sun Q, Gu P. Modeling of Bond Formation Between Polymer Filaments in the Fused Deposition Modeling Process. *J Manuf Process*. 2004;6(2). doi:10.1016/S1526-6125(04)70071-7

24. Seppala JE, Hoon Han S, Hillgartner KE, Davis CS, Migler KB. Weld formation during material extrusion additive manufacturing. *Soft Matter*. 2017;13(38). doi:10.1039/C7SM00950J

25. Bhalodi D, Zalavadiya K, Gurrala PK. Influence of temperature on polymer parts manufactured by fused deposition modeling process. *J Brazilian Soc Mech Sci Eng*. 2019;41(3). doi:10.1007/s40430-019-1616-z

26. Gurrala PK, Regalla SP. Part strength evolution with bonding between filaments in fused deposition modelling. *Virtual Phys Prototyp*. 2014;9(3). doi:10.1080/17452759.2014.913400

27. Coogan TJ, Kazmer DO. Healing simulation for bond strength prediction of FDM. *Rapid Prototyp J*. 2017;23(3). doi:10.1108/RPJ-03-2016-0051

28. Coogan TJ, Kazmer DO. Prediction of interlayer strength in material extrusion additive manufacturing. *Addit Manuf*. 2020;35. doi:10.1016/j.addma.2020.101368

29. McIlroy C, Olmsted PD. Disentanglement effects on welding behaviour of polymer melts during the fused-filament-fabrication method for additive manufacturing. *Polymer (Guildf)*. 2017;123. doi:10.1016/j.polymer.2017.06.051

30. Yin J, Lu C, Fu J, Huang Y, Zheng Y. Interfacial bonding during multi-material fused deposition modeling (FDM) process due to inter-molecular diffusion. *Mater Des*. 2018;150. doi:10.1016/j.matdes.2018.04.029

31. Zhang X, Wang J. Controllable interfacial adhesion behaviors of polymer-on-polymer

surfaces during fused deposition modeling 3D printing process. *Chem Phys Lett*. 2020;739. doi:10.1016/j.cplett.2019.136959

32. Ko YS, Herrmann D, Tolar O, Elspass WJ, Brändli C. Improving the filament weld-strength of fused filament fabrication products through improved interdiffusion. *Addit Manuf*. 2019;29. doi:10.1016/j.addma.2019.100815

33. Patterson AE, Chadha C, Jasiuk IM, Allison JT. Design and repeatability analysis of desktop tool for rapid pre-cracking of notched ductile plastic fracture specimens. *Eng Fract Mech*. 2019;217. doi:10.1016/j.engfracmech.2019.106536

34. Jasiuk I., Abueidda I.D., Kozuch C, Pang S, Su F, McKittrick J. An overview on additive manufacturing of polymers. *Journal of the Minerals, Metals and Materials Society*(2018) 70 (3), 275-283. doi: 10.1007/s11837-017-2730-y